mathematics

MDPI

Article

Segmentation and Analysis Emphasizing Neonatal MRI Brain Images Using Machine Learning Techniques

Saritha Saladi [1], Yepuganti Karuna [2], Srinivas Koppu [3], Gudheti Ramachandra Reddy [2], Senthilkumar Mohan [3], Saurav Mallik [4,*] and Hong Qin [5,*]

[1] School of Electronics Engineering, VIT-AP University, Vijayawada 522237, India
[2] SENSE, Vellore Institute of Technology, Vellore 632014, India
[3] School of Information Technology and Engineering, Vellore Institute of Technology, Vellore 632014, India
[4] Department of Environmental Health, Harvard T H Chan School of Public Health, Boston, MA 02115, USA
[5] Department of Computer Science and Engineering, University of Tennessee at Chattanooga, Chattanooga, TN 37403, USA
* Correspondence: sauravmtech2@gmail.com or smallik@hsph.harvard.edu (S.M.); hong-qin@utc.edu (H.Q.)

Abstract: MRI scanning has shown significant growth in the detection of brain tumors in the recent decade among various methods such as MRA, X-ray, CT, PET, SPECT, etc. Brain tumor identification requires high exactness because a minor error can be life-threatening. Brain tumor disclosure remains a challenging job in medical image processing. This paper targets to explicate a method that is more precise and accurate in brain tumor detection and focuses on tumors in neonatal brains. The infant brain varies from the adult brain in some aspects, and proper preprocessing technique proves to be fruitful to avoid miscues in results. This paper is divided into two parts: In the first half, preprocessing was accomplished using HE, CLAHE, and BPDFHE enhancement techniques. An analysis is the sequel to the above methods to check for the best method based on performance metrics, i.e., MSE, PSNR, RMSE, and AMBE. The second half deals with the segmentation process. We propose a novel ARKFCM to use for segmentation. Finally, the trends in the performance metrics (dice similarity and Jaccard similarity) as well as the segmentation results are discussed in comparison with the conventional FCM method.

Keywords: MRI segmentation; histogram equalization; CLAHE; BPDFHE; neonatal brain; ARKFCM; FCM

MSC: 26E50; 62A86; 03B52; 93C42; 60A86

check for updates

Citation: Saladi, S.; Karuna, Y.; Koppu, S.; Reddy, G.R.; Mohan, S.; Mallik, S.; Qin, H. Segmentation and Analysis Emphasizing Neonatal MRI Brain Images Using Machine Learning Techniques. *Mathematics* **2023**, *11*, 285. https://doi.org/10.3390/math11020285

Academic Editor: Junseok Kim

Received: 23 November 2022
Revised: 20 December 2022
Accepted: 22 December 2022
Published: 5 January 2023

1. Introduction

MRI segmentation is a technique that deals with magnetic resonance imaging using low energy waves with wavelengths higher than X-rays and infrared rays along with a magnetic field to get a pictorial view of the anatomy of different body parts. The image is further classified based on similarity measures for ease of result analysis. MRI is eminently convenient in providing 3D visualization and anatomy of the brain. It can be represented in both 2D (pixels) and 3D (voxels). Although there are other imaging techniques, e.g., X-rays, CT, PET, SPECT, etc., X-rays and CTs (computed tomography) involve the use of mild radiation and prolonged exposure to neonates, which can be fatal. As long as functional behavior of the brain is not a requisite, MRI is better than other modalities. On the contrary, a modified version of MRI called fMRI (functional magnetic resonance imaging) aids in the visualization of sheer suddenness in neural activity of the brain corresponding to a particular stimulus. The above-presented information stands for the remarkable growth of MRI specifically.

This paper is focused on the analysis of neonatal brains, i.e., the brains of infants. The main difference between the brains of a neonate and a matured one is that mature brain tissues are comprised of white matter (WM), grey matter (GM), and cerebro-spinal fluid (CSF) whereas neonate brain tissues contain additional myelinated and nonmyelinated white matter tissues, which are nothing but fatty tissues that help in the development of the brain. These fatty tissues greatly affect the segmentation process as they create overlaps between different tissue classes, e.g., WM–GM overlaps dominate the GM–CSF overlaps, which may lead to inaccurate results, i.e., ambiguous boundary decisions become liable outcomes between various tissue class distributions. Hence, proper enhancement of the image becomes indispensable before segmentation is carried out. Preprocessing involves skull stripping, image enhancement, artifact removal, and noise removal. The prevalent noises in MR images follow Rician distribution in general. Preprocessing eliminates difficulties produced due to bias fields, which are nothing but lower frequency multiplicative fields and are neglected if the MRI is performed on a comparatively lower magnetic field strength, e.g., around 0.5 Tesla and increasing (incrementing it to 2T/3T or above), which can make the bias field significant and ultimately affect the outcome of the MRI process. To provide a general estimation, MRI scanning uses a magnetic field that is roughly around 8000 times the magnetic field of the earth. The use of support vector machines (SVMs) and fuzzy c-means (FCM) algorithms are the most common algorithms for segmentation. Both of the above-mentioned algorithms are unsupervised machine learning algorithms. The former is germane to statistical learning theory while the latter does an exemplary genesis of clusters and solves skeptical problems existing in an image. As we all know, everything has pros and cons. The above algorithms also have some cons. SVM is unable to segregate categorical data of ambiguous samples.

In order to overcome the demerits of the FCM algorithm for MRI brain images and enhance the images with preprocessing techniques, both were combined together to improve the accuracy of the output. In this paper, an adaptively regularized kernel-based fuzzy c-means (ARFKCM) algorithm is proposed for the segmentation technique for preprocessed images. To avoid inaccurate results, various preprocessing techniques, such as HE, CLAHE, and BPDFHE, were analyzed, and the best method for preprocessing was chosen based on performance metrics such as MSE, PSNR, RMSE, AMBE, and so on. After preprocessing the original image, segmentation was performed on the preprocessed image. Finally, the abnormality was depicted in the results of the preprocessed, segmented image and in the one without. This paper implements an intensity-based segmentation method (which includes region growth, classification, clustering, and thresholding). In the case of the FCM algorithm, the clustering membership function was determined by the similarity between the cluster center and the pixel intensity, and not considering the spatial dependence of the pixels makes it extremely responsive to noise and Euclidean space. This paper is summed up as follows: In Section 2, under materials and methods the literature of existing methods and proposed methods are described. Section 3 explores the experimental results, the discussion on the results and their comparisons with existing methods is shown Section 4, and the conclusion is described in Section 5.

2. Materials and Methods

2.1. Literature Review

The proposed work is motivated by the fact that the most difficult task of MRI brain imaging is to eliminate noise from the scanning modality in the acquired images. Another challenge in the segmentation of MRI images is due to the presence of noise and ambiguities between boundaries and dissimilar tissues in the brain. The segmentation of tumors is due to structural divergences due to an assortment in shape, dimension, and position of the tumor present in the brain. Additionally, subjects can be resourcefully evaluated within the shortest time duration by reducing the valuable time and energy of a radiologist in the diagnosing process. The proposed hybrid techniques enable the accurate detection of tissue and tumor areas with their exact topology, which is typically unknown to a radiologist.

Lakshmi A. et al. [1] were enthralled by preprocessing various stages, such as artifact removal, image enhancing, and skull stripping. In the end, the noise was successfully removed from the MR image, and curvelet transformation was used to do it. Senthilkumaran N and Thimmiaraja J [2] focused on the analysis and assessment of dissimilar histogram equalization techniques, i.e., brightness-preserving dynamic histogram equalization (BPDHE), global histogram equalization (GHE) [3], adaptive histogram equalization (AHE), and local histogram equalization (LHE), based on parameters such as Michelson contrast, Weber contrast, contrast, and AMBE.

They introduced fuzzy theory into the prevalent algorithm and also a better technique known as brightness-preserving dynamic fuzzy histogram equalization (BPDFHE). The inexactness of grey level values was handled to a large extent with fuzzy statistics of digital images, resulting in improved performance.

Suryavamsi et al. [4] performed a deep analysis of image enhancement methods (HE, CLAHE, and BPDFHE) on astrocytoma MR images. In the results, BPDFHE performed exceptionally well compared to HE and CLAHE based on performance measures such as MSE, RMSE, and PSNR. This paper explores different methods for various sample images. Deep et al. [5] performed a comparative analysis of the different types of contrast enhancement techniques on dissimilar images and other denoising algorithms used for preprocessing as used in [6]. In the conclusion, contrast-limited adaptive histogram equalization obtained better image quality.

Sai Raghavendra et al. [7] proposed the implementation of a multiplicative intrinsic-component optimization (MICO) methodology to both single and multichannel MRI images for segmenting multiple sclerosis lesions.

Ivana Despotovic et al. [8] analyzed the famous methods generally used for brain MRI segmentation to address their complexity and challenges, and other segmentation methods were discussed. Various MRI preprocessing steps were described, including bias field correction. The advantage, capabilities, differences, and limitations related to the topic were described with simulated illustrations of histograms as well as manual segmentation, atlas-based, intensity-based, surface-based, and hybrid segmentation methods.

Saritha Saladi and Amutha Prabha N [9] presented various segmentation methods such as manual, semiautomatic, fully automatic, and hybrid segmentation in a detailed manner and stated that hybrid methods can overcome the limitations of individual methods. Shijuan He et al. [10] proposed methods for finding brain contours along with the formulation of real calculation models.

The following papers show the recent works related to the machine learning domain, emphasizing how segmentation can be improved using various combinations of famous algorithms, such as fuzzy theory and SVMs. Xiao and Tong [11] explained FCM and FSVM. Membership points were selected in FSVM algorithm, where as FSM algorithm selects blur membership points. This process not only added the unheard FCM algorithm to the monitored SVM classification algorithm so it can automatically select patterns for the SVM algorithm but also made better use of the FCM algorithm's generalization capability compared to normal SVM to achieve better accuracy in segmentation.

Dancea [12] introduced a format separation technique in conjunction with FCM and FSVM to solve the training problem for the shortage of models, which proposed an improved FCM algorithm with SVM. Additionally, [13–15] combined FCM and SVM to diagnose osteoarthritis of the knee. Satya [16] promoted a better and more effective KFCM technique in conjunction with SVM for breast MR image segmentation. Elazab and Wang [17] proposed ARKFCM and were able to achieve a trade-off between high-segmentation accuracy and low computational cost.

Thejaswini, P. et al. [18] usedwere ARKFCM for segmentation, and SVM and ANN are proposed for the detection and classification of brain tumors based on the extracted features. Iqbal et al. and Zhu et at. [19,20] used a deep convolutional neural network to segment brain tumors in MRIs in their paper. The three different network architectures were interpolated network, Skip-Net, and SE-Net. It was concluded that VGG architecture performs well for tumor segmentation.

Akkus et al. [21] reviewed the current deep learning architectures (patch-wise, semantic-wise, and cascaded CNN) used for the segmentation of anatomical brain structures and brain lesions, and their performance, speed, and properties were summarized and discussed.

Zahid Ullaha et al. [22] proposed a preprocessed method for brain MRI classification using histogram equalization, median filter, color moments, DWT, ANN, etc. This method performed better than the preexisting method in terms of accuracy, classification, and computation time, as feature reduction and image enhancement were accomplished beforehand. The following image represents the flow of processes in the process, which is shown in Figure 1, and their corresponding algorithms are discussed in detail.

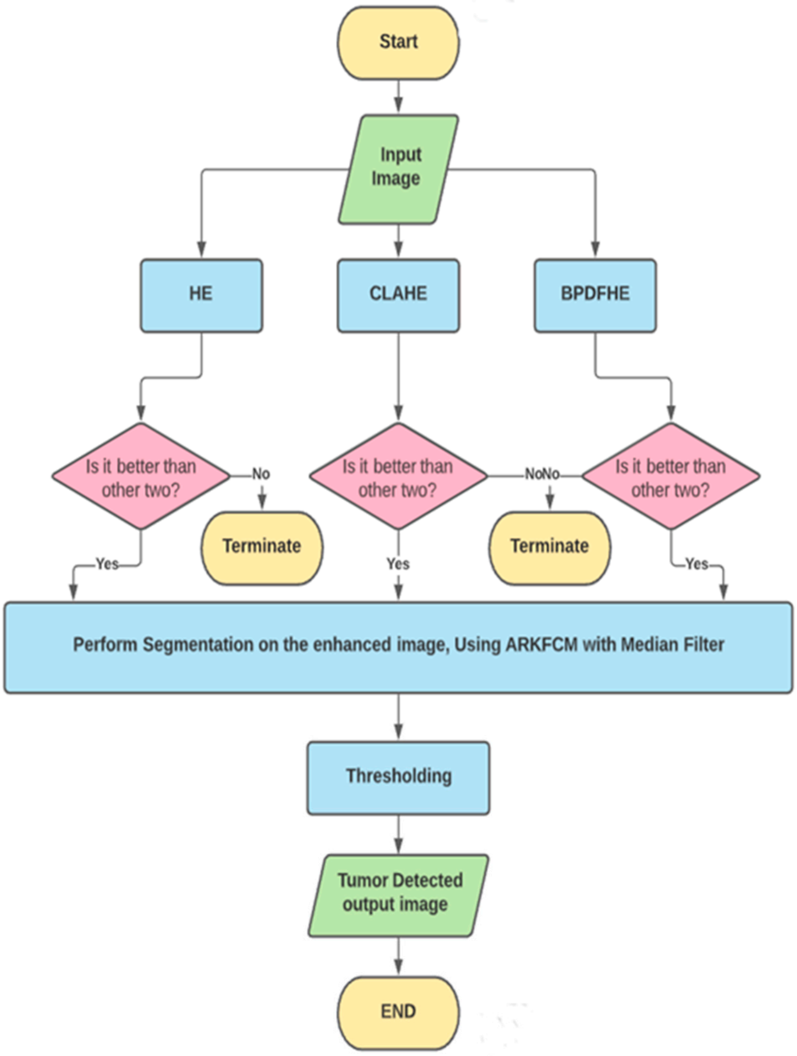

Figure 1. Block diagram of the proposed system with ARKFCM algorithm.

2.2. Preprocessing of the Original Image

Preprocessing was carried out using three different enhancement techniques, namely HE, CLAHE, and BPDFHE.

2.2.1. Histogram Equalization (HE)

HE is a technique used to improve the contrast of an image. This is accomplished by stretching out the intensity range of the image. The regions of lower local contrast gain the highest contrast. HE is a statistic probabilistic distribution of every gray level in images. The algorithmic steps to find the HE are as follows:

(a) Evaluate probability distribution function (PDF). Let the input images contain N discrete gray levels from $[0, N-1]$. Then, PDF is calculated by: $p[x_N] = \frac{pixel\ having\ intensity\ (x_N)}{total\ number\ of\ pixels}$, $p[x_N] = \frac{n\ (x_N)}{r*c}$. Here, r represents the number of rows, c represents the number of columns, and $n(x_L)$ represents the count of pixels with intensity x_L.
(b) Calculate the cumulative distributive function (CDF). This is performed by adding all the calculated PDF values, $\mathrm{A}[x_N] = \sum_{\mathrm{i}=0}^{\mathrm{M}} p[x_i]$, where $\mathrm{M} \in [0, \mathrm{M}-1]$.
(c) Evaluate the transfer function. This is performed by multiplying the obtained CDF value by the number of grey levels, $\mathrm{T}[x_N] = (\mathrm{M}-1)\ \mathrm{A}[x_N]$.
(d) Map the obtained intensity values with previous intensity values.

Hence, the image is enhanced, and its corresponding equalized histogram is obtained.

2.2.2. Contrast-Limited Adaptive Histogram Equalization (CLAHE)

In this method, the images are divided into small blocks called tiles, and each of the tiles is histogram equalized. With this method, noise amplification is avoided in the image. The adjacent tiles are merged using bilinear interpolation to separate the artificial boundaries. Each of the tiles is enhanced separately to obtain the required histogram for the given parameters. All secondary images are combined to obtain a well-developed image. A new framework that is introduced in CLAHE is the clip limit, which limits the augmentation by clipping the histogram with the help of given parameters. The following steps are used in CLAHE:

(a) Divide the given input image into various subimages.
(b) On the obtained sub images in (a), the following steps are performed on each bin in the histogram of the subimage once the biggest value of that bin is acquired:
   - If specified clip value is smaller than the histogram bin value, then the histogram will be clipped to the clip value.
   - Evaluate the number of pixels where bin values exceed the given clip value.
(c) Redistribute the above pixels to other histogram bins evenly to obtain the normalized histogram.
(d) After obtaining the normalized histogram, find the CDF values.
(e) For every pixel of the given image, find the neighboring pixels.
(f) By using the intensity of pixel values, map those neighboring pixels based on the above-calculated CDF values.
(g) The obtained pixel values are mapped based on the new intensity values in the given $[0, N-1]$ range.

2.2.3. Brightness-Preserving Dynamic Fuzzy Histogram Equalization (BPDFHE)

The BPDFHE method operates using an image histogram in such a way that redistribution of the gray level takes place. It is a general modification of BPDHE to lessen its computational complexity and upgrade its contrast enhancement and brightness-preserving abilities. BPDFHE uses fuzzy statistics of digital images for their representation and processing. Involving the fuzzy domain enables the technique to steer the impreciseness of gray level values in a superior way and yields a better execution. The algorithmic steps are as follows:

(a) Fuzzy histogram computation;
(b) Partitioning of the histogram;
(c) Dynamic histogram equalization of the partitions;
(d) Normalization of the image brightness.

2.3. Results of Performance Metrics in Preprocessing

The eminence of an image is subjective; it differs from image to image. The following measures are used to evaluate the preprocessing task (HE, CLAHE, and BPDFHE):

2.3.1. Mean Square Error (MSE)

Mean square error (MSE) is defined as the ratio of the input image matrix and enhanced image matrix. It is the cumulative squared error between the primary and retrieved images. If the MSE value is smaller, the probability of error is low.

$$MSE = \frac{\Sigma_{mn}[J_1(m,n) - J_2(m,n)]^2}{M \times N} \tag{1}$$

where J_1—original image and J_2—compressed image with $M \times N$ dimensions. Therefore, lower values of MSE lead to effective compression.

2.3.2. Peak Signal-to-Noise Ratio (PSNR)

Peak signal-to-noise ratio (PSNR) is defined as the ratio of the logarithmic peak value of a given image to the logarithmic MSE value. It is typically used as an extent of the standard of restoration after lossy compression. The higher the PSNR value, the lower the error will be, and this results in a good-quality image.

$$PSNR = 10\log_{10}\left(\frac{A^2}{MSE}\right) \tag{2}$$

where A—highest possible value of the image's pixel.

2.3.3. Root Mean Square Error (RMSE)

RMSE is calculated by taking the square root of the mean square error value. The similarity between the two images will be calculated. If RMSE is zero, then the two images are equal. The lesser the value of RMSE, the lower the value of error.

$$RMSE = \sqrt{MSE} \tag{3}$$

2.3.4. Absolute Mean Brightness Error (AMBE)

AMBE is considered the difference between the mean of the given image and the enhanced image.

$$\text{AMBE} = |\,\mathrm{E}(J_1) - \mathrm{E}(J_2)\,| \tag{4}$$

$\mathrm{E}(J_1)$—expectation(mean) of the original image and $\mathrm{E}(J_2)$—expectation of the compressed image. The lower the value of AMBE, the better the performance of the brightness-preserving factor to improve the quality of the output image.

2.4. Segmentation of Images

The most common algorithms for this purpose are FCM, SVM, and random forest ada-boost m1 classifier SVM and MRF [23], all of which are well-known machine learning algorithms. The former two are unsupervised clustering methods whereas the latter is a supervised one such as the firefly and k-means algorithms [24].

Clustering and segmentation both aim at assembling entities based on their similarities, but clustering allocates valued scores to clusters in order to make the objects in the same cluster as analogous as possible and vice versa. Clusters are identified based on similarities, such as connectivity, distance, and intensity. Segmentation [25] of an image implies that an image should be divided into a set of identical substantial, uniform, and non-overlapping areas consisting of analogous characteristics, e.g., intensity, depth, color/gradient. The resulting image must provide us with a labeled outcome of homogeneous spatial contexts or curves representing field boundaries.

2.4.1. Fuzzy C-Means Clustering

FCM is known as soft clustering [26] and segments data groups into many clusters. This method deals with an objective function that, via iteration, allocates a membership value to each pixel in the image. The extent of the membership value highly depends on the distance of a particular pixel from the centroid of a cluster. In general, more data near the cluster center implies a greater membership value towards the particular cluster center and vice versa. Hence, the summation of the membership values of each point should be equal to one. The processes executed in basic FCM are summarized in Figure 2.

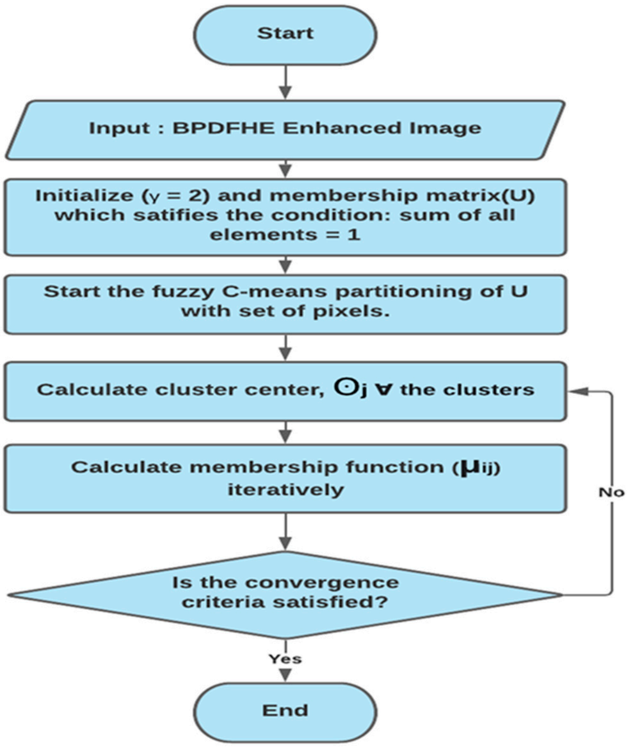

Figure 2. Flowchart for FCM algorithm.

Apart from these, FCM has some hindrances:

- JFCM ignores the dimensional dependence among the pixels of the input sample and deals with images that are the same as isolated points.
- By ignoring the provincial information, the algorithm becomes extremely sensitive to noise. Hence, MR images comprising noise and nonuniform intensity result in erroneous segmentation.

To make the algorithm insusceptible to noise, the following modification was established, and the improved algorithm was termed FCM_S by Ahmed et al. [25]. The objective function pertinent to the refashioned algorithm is given as:

$$J_{FCM\_S} = \sum_{i=1}^{n}\sum_{j=1}^{c}\mu_{ij}^{\gamma}\|\rho_i - \odot_j\|^2 + \alpha\sum_{i=1}^{n}\sum_{j=1}^{c}\mu_{ij}^{\gamma} * \frac{1}{n_c}\left(\sum_{x\in n_i}\|\rho_x - \odot_j\|^2\right) \quad (5)$$

- Here, 'α' acts as a controlling parameter within range [0, *N*]. It is the local dimensional information. Further apprehension on this parameter is provided in Section 2.5.2 of this paper.
- 'n_i'—set of pixels in the neighborhood of the ith pixel.
- 'n_c'—count of the elements in the n_ith set.

The complex-computations of the FCM_S algorithm is high, in order to avoid the complex-computations last part of the second term, i.e., $\frac{1}{n_c}\left(\sum_{x\in n_i}\|\rho_x - \odot_j\|^2\right)$. Here, 'ρ' is a grayscale of the enhanced image and needs to be predetermined; replacement of the Euclidean distance with the kernel function was accomplished in paper [27]. Average and median filters were used to redesign the algorithm, and the improved versions are termed FCM_S1 and FCM_S2.

Further remodeling was attained multiple times with this algorithm. Paper [28] innovated two forms, i.e., GKFCM1 and GKFCM2, which were the intensification of FCM_S1 and FCM_S2, respectively, and had a new Gaussian kernel-based parameter that replaced α and yielded better results but had complications in case the cluster centers were compact. This resulted in increased iteration extensively.

The above complication was eradicated by the introduction of the FLICM algorithm in paper [29] that used fuzzy theory to make it robust to noise. Again, the problem of losing minute specifications with the KW-FLICM algorithm, which exchanged Euclidean distance with the kernel-based function but at the price of losing fuzzy factors, again encountered the escalation of iterations.

Szilagyi [30] exposed the blunders of the above two algorithms—FLICM and KW-FLICM. Their theoretical flaws were questioned and declared unsuitable. These facts lead the researchers back to square one and explicated the process thereafter.

2.4.2. Markov Random Fields

It is also one of the popular segmentation methods. Similar to FCM, MRF is also an unsupervised clustering algorithm. It shows exemplary performance when capturing local spatial interactions, and pixel (or voxels in the case of 3D) intensity is required. It provides both 2D and 3D spatial configurations. According to the neighborhood relationship properties:

- A node does not belong in its neighborhood,
- A mutual relationship exists in a neighboring relationship.

According to these properties, we can understand from the illustration that four neighbors exist for a node of a 2D image in first order, and six exist in the case of a 3D image. Similarly, in second order, eight exist for 2D and 18 neighbors exist for. Following the same, neighbors for third order for both 2D and 3D can be visualized.

2.4.3. Support Vector Machines

It is a widely used supervised machine learning method. It uses statistical theory by the virtue of which kernel functions extrapolate data into higher spatial dimensions to achieve ease of their separation. This process also gets aided by a kernel trick that uses the dot product to efficiently transform a linear algorithm into a nonlinear algorithm. Apart from the pros, it also has a con: As far as ambiguous samples are concerned, its partitioning capability becomes limited, and it fails to categorize the data for the corresponding sample.

2.5. Proposed Methodology

2.5.1. Highlights of the Proposed Method

MRI images are distorted by noise at the time of acquisition, which reduces the attributes and limits the accurateness in analysis. Elimination of noise in medical images is an essential task in preprocessing, and there are various approaches.

In this paper, various denoising algorithms are compared with the proposed ARKFCM method to exterminate the noise in MRI images with a pixel restoration process. The qualified assessment of this technique was carried out with the help of metrics (PSNR, MSE, RMSE [31], and AMBE [32]). These comparisons show that the BPDFHE filter provides outstanding performance in terms of improved PSNR and RMSE in perceptual interpretation. It supports in the medical diagnosis of brain disorders.

There are various challenges to solving the inequities during the image acquisition process in the detection of tumors and segmenting of tissues (GM, WM, and CSF). The transparency and interpretation in the hybrid segmentation methods are a noteworthy challenge for clinical approval from doctors.

To provide better tumor identification and tissue segmentation with the hybridization of the algorithms and to overcome the limitations of the individual segmentation methods, a combination of different segmentation methods is proposed with the ARKFCM technique.

2.5.2. Adaptive Regularized Kernel-Based Fuzzy C-Means Clustering Algorithm (ARKFCM)

The overview of this algorithm is shown in the Figure 3 associated with this section. Here, the term 'adaptive regularization' indicates the existence of the adaptive calculation of 'α', a parameter used during the modification of FCM, making it resilient to high noise levels. This 'α' influences the algorithm's performance to a great extent. The prerequisite in case of FCM for this parameter was that it had to be specified by the concerned programmer himself for which prior knowledge of the details of the noise becomes an obligation. Considering scrutiny over the bulk of the dataset, it becomes immensely challenging, time consuming, and counterproductive to calculate α for each pixel, as noise levels vary window per window. The above is the case when prior information about the noise is available, which contradicts the general case. In general, the noise information prevailing in a sample remains unknown, which adds to the limitations of FCM. Hence, this algorithm performs a computation for the value of α before commencing any actual operation in order to be adaptive to the level of pixel noise.

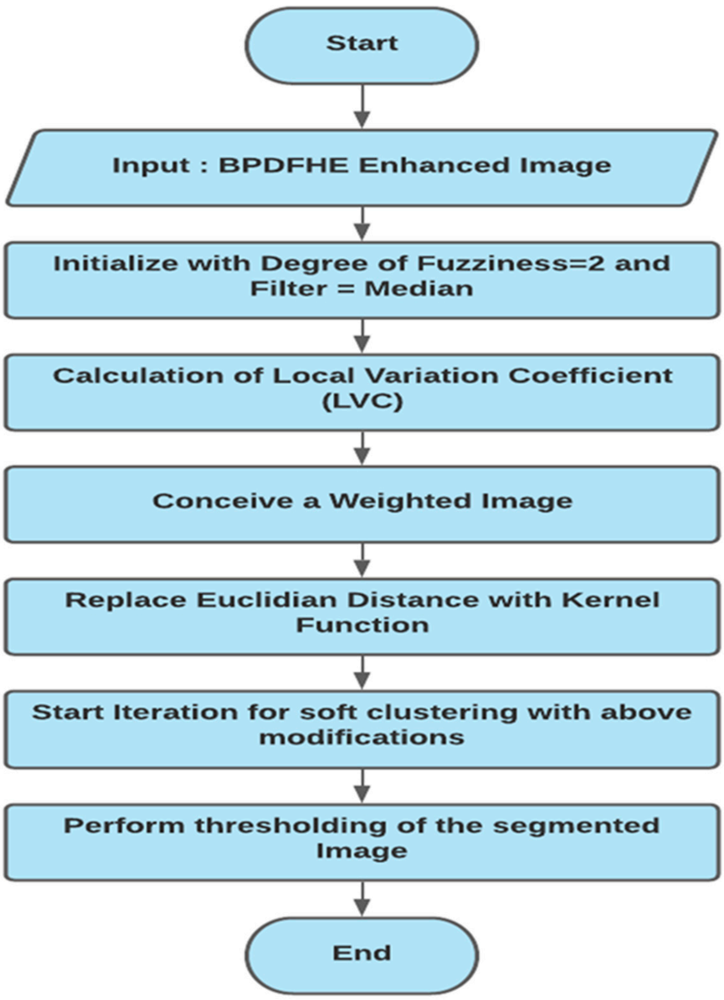

Figure 3. Flowchart of Segmentation (ARKFCM followed by thresholding) Process.

Initialization

Because of the contributing factor of 100% noise reduction, the median filter is accomplished over a weighted filter even if the filter mask is heightened. Another feature of the median filter is that the obscuring nature of the outcome is less compared to the other two. The degree of fuzziness is the weighting exponent on all fuzzy memberships.

Local Variation Coefficient Calculation

The LVC calculation becomes a requisite as it approximates the divergence (if any) present in a particular pixel's neighborhood window. A pixel that has been picked randomly to find the local variable coefficient. It is given as:

$$\mathrm{LVC} = \frac{\sum_{z \in n_i} (\rho_z - \overline{\rho_i})^2}{n_c (\overline{\rho_i})^2} \tag{6}$$

Here, 'ρ_z' is a random pixel in the ith pixel neighbor. 'n_i' is the set of pixels in the ith pixel neighbor. 'n_c' is the count of the elements in the n_ith set. The results of windowing operations on pixels are modeled as random variables, so we treat the pixel as a random variable in the calculation of local variables.

Thereafter, the LVC for the window of the ith pixel is further applied to the exponential function to derive the weights within that particular dimensional neighborhood, i.e., the window associated with that pixel.

$$\delta_i = \frac{\xi_i}{\sum_{z \in n_i} \xi_z} \tag{7}$$

where $\xi_i = e^{(\sum_{z \in n_i,\ i \neq z} LVC_Z)}$

The above expression indicates that for all pixels 'i', the values of δ_i rise whenever the summation of the local variation coefficients in the surrounding of the ith pixel is large and vice versa.

A new parameter 'Ψ' is introduced at this step to allot larger values to the pixels possessing higher LVC values. It replaces the term 'α' by the virtue of which 'adaptive regularisation' is achieved. The weight is allocated to each pixel based on the following function:

$$\Psi_i = \begin{cases} 2 + \delta_i, & \overline{\rho_i} < \rho_i \\ 2 - \delta_i, & \overline{\rho_i} > \rho_i \\ 0, & \overline{\rho_i} = \rho_i \end{cases} \tag{8}$$

From this expression, we can conclude that whenever the ith central pixel (ρ_i) is brighter than the average grayscale ($\overline{\rho_i}$) of the pixels in its local window, a higher weight is assigned to the corresponding pixel. The converse of the preceding statement is also evident from the second case of the above expression. Finally, if the grayscale of the central pixel is identical to the local average (i.e., $\overline{\rho_I} = I$), then this algorithm would become equivalent to the conventional FCM algorithm. Hence, adaptive regularisation is attained using Ψ_i.

Conceiving a Weighted Image

This is an optional step where it is at the researcher's discretion of weighted images using 'Ψ' or to go for any of the filters—median/average. The limitation in the former choice is that it becomes highly challenging when one wants to exclude all other parameters except for one.

Use of Kernel-Based Function

Despite being a fundamental method and with low complexity in computation, Euclidean distance does have a complication, i.e., it is sensitive to aberrations caused by outside influences. To eradicate this sensitivity to deviations, a kernel-based function is used instead, which is an application of support vector machines. The kernel function is given as:

$$K(\rho_i, \odot_j) = e^{\frac{-\|\rho_i - \odot_j\|^2}{2\theta^2}} \tag{9}$$

where $\theta = \sqrt{\left[\frac{\sum_{i=1}^{n}\left(\delta_i-\bar{\delta}\right)^2}{n-1}\right]}$.

Iterations: Iterations are carried out based on the soft clustering algorithm. Overall, the objective function of ARKFCM including all specifications is given as:

$$J_{\mathrm{ARKFCM}} = 2\left[\sum_{i=1}^{n}\sum_{j=1}^{c}\mu_{ij}^{\gamma}\left(1-K\left(\rho_i,\odot_j\right)\right)+\sum_{i=1}^{n}\sum_{j=1}^{c}\Psi_i\mu_{ij}^{\gamma}\left(1-K\left(\overline{\rho_i},\odot_j\right)\right)\right] \quad (10)$$

The above equation is a transformation of Equation (10) achieved by modifications mentioned in the algorithm of ARKFCM. Similarly, the cluster centers and membership function is derived as in the conventional FCM algorithm [15]. Finally, thresholding is performed on the resulting segmented image, i.e., all pixels above the specified value are turned black and vice versa for white, which helps in visualizing tumors (if any) present in the neonatal brain.

3. Results

The following are the results after analyzing the preprocessing techniques based on performance metrics such as MSE, PSNR, RMSE, and AMBE.

3.1. Preprocessing Results

The following figures are the enhanced images with their corresponding histograms (HE, CLAHE, and BPDFHE) for the original images.

Figure 4a is the original. Figure 4b is its histogram representation. Figure 5a–c represents the same image enhanced via different preprocessing methods, i.e., HE, CLAHE, and BPDFHE, and Figure 6a–c is their respective histograms.

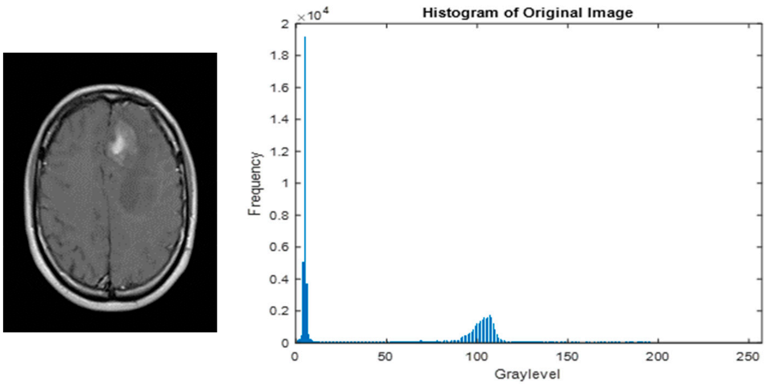

(**a**) (**b**)

Figure 4. (**a**) Original Image; (**b**) Histogram Image.

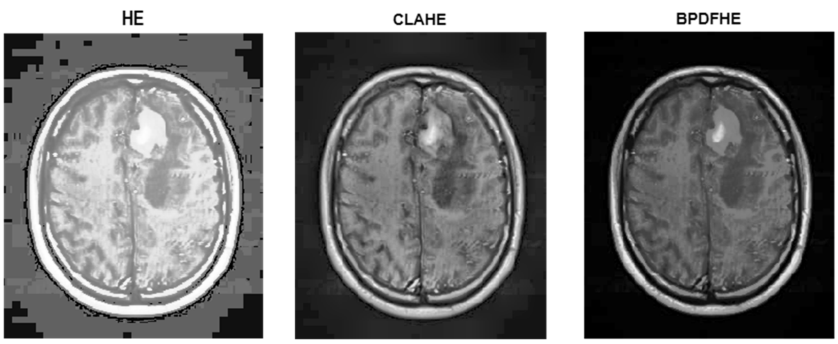

(**a**) (**b**) (**c**)

Figure 5. Preprocessed with (**a**) HE, (**b**) CLAHE, and (**c**) BPDFHE.

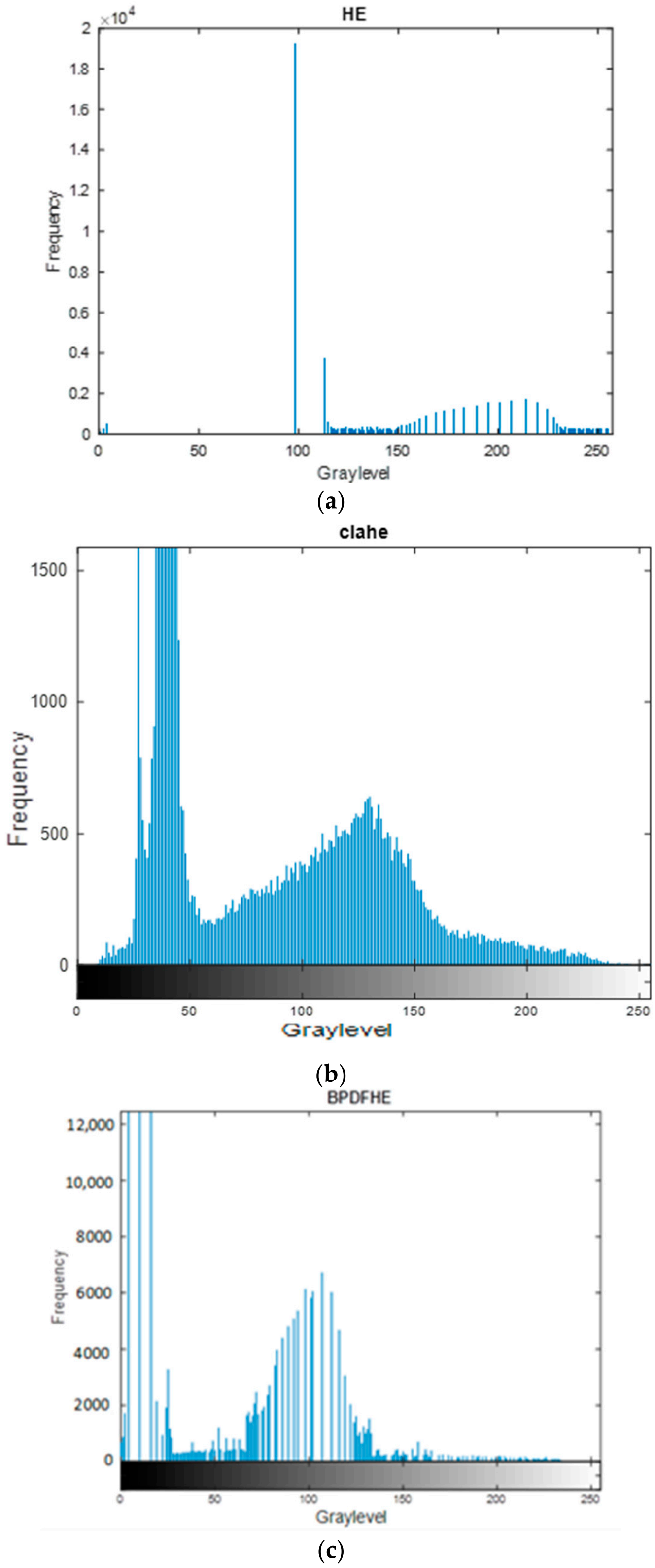

Figure 6. Histograms of preprocessed images of Figure 5. (**a**) HE, (**b**) CLAHE, and (**c**) BPDFHE.

Figure 7a is the original image. Figure 7b is its histogram representation. Figure 8a–c represents the same image enhanced via different preprocessing methods, i.e., HE, CLAHE, BPDFHE, and Figure 9a–c is their respective histograms.

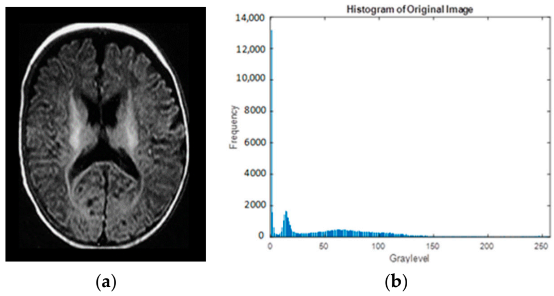

Figure 7. (**a**) Original Image; (**b**) Histogram Image.

Figure 8. Preprocessed with (**a**) HE, (**b**) CLAHE, and (**c**) BPDFHE.

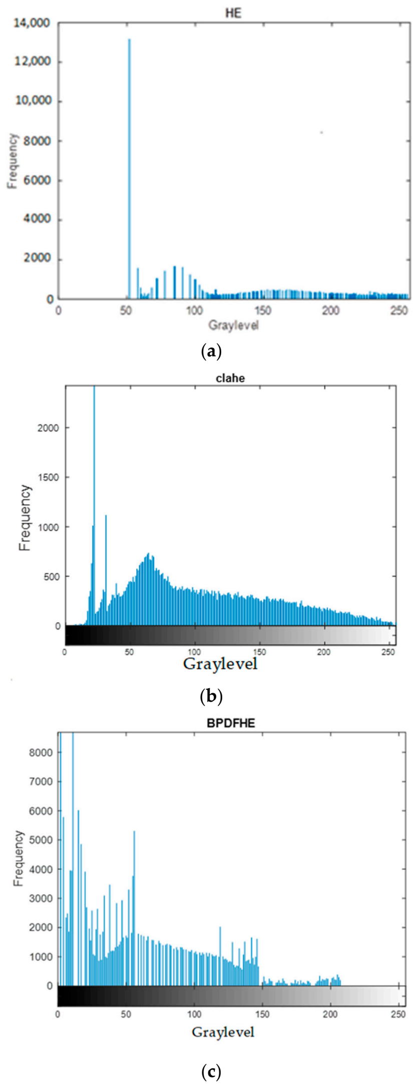

Figure 9. Histograms of preprocessed images of Figure 8. (**a**) HE, (**b**) CLAHE, and (**c**) BPDFHE.

3.1.1. Mean Square Error (MSE)

The MSE results were assessed for 10 neonatal brain images utilizing the three enhancement procedures. With the help of Table 1, we can interpret the pattern of the MSE values. On average, the MSE value lowered by 63.21% from HE to CLAHE, dropped to 97.55% from HE to BPDFHE, and decreased by 94.75% from CLAHE to BPDFHE. The value for BPDFHE is lower than the other two, implying it has a low error and yields a more desirable image.

Table 1. Comparison of MSE values.

S.no.	HE	CLAHE	BPDFHE
Image 1	6998	2081.3	47.4052
Image 2	7344.8	2171.1	108.6676
Image 3	5565.2	1929.3	63.7714
Image 4	1241.3	1373.2	167.8926
Image 5	5375.1	1645.5	42.4575
Image 6	3833.1	1156.3	66.5487
Image 7	7188.8	2084.3	95.3092
Image 8	10312	3265.4	96.8685
Image 9	6034.4	1143	97.3825
Image 10	5169.3	1185.7	63.3049

3.1.2. Peak Signal-to-Noise Ratio

The PSNR results were assessed for 10 neonatal brain images utilizing the three enhancement techniques. With the help of Table 2, we can interpret the pattern for the PSNR values. On average, the PSNR value increased by 44.95% from HE to CLAHE, raised to 66.9% from HE to BPDFHE, and further increased by 84.177% from CLAHE to BPDFHE. The value for BPDFHE is high, which infers it has a low error and yields a more desirable image.

Table 2. Comparison of PSNR values.

S.no.	HE	CLAHE	BPDFHE
Image 1	9.6811	14.9475	31.3725
Image 2	9.471	14.7641	27.7698
Image 3	10.676	15.2767	30.0845
Image 4	17.192	16.7535	25.8805
Image 5	10.8269	15.9679	31.8513
Image 6	12.2953	17.4999	29.8994
Image 7	9.5643	14.9411	28.3395
Image 8	7.9973	12.9914	28.269
Image 9	10.3245	17.5502	28.246
Image 10	10.9964	17.391	30.1164

3.1.3. Root Mean Square Error

The RMSE results are evaluated for 10 neonatal brain images using the three enhancement techniques. Table 3 helps to interpret the trend of MSE values. On average, RMSE value drops by 41.5% from HE to CLAHE, again falls by 86.51% from HE to BPDFHE, and furthermore by 77.84% from CLAHE to BPDFHE. The value for BPDFHE is less suggesting that it has a low error and provides us with a better-quality image.

Table 3. Comparison of RMSE values.

S.no.	HE	CLAHE	BPDFHE
Image 1	83.6539	45.6212	6.8851
Image 2	85.7019	46.5945	10.4244
Image 3	74.6003	43.9241	7.9857
Image 4	35.232	37.0564	12.9573
Image 5	73.3151	40.5643	6.5159
Image 6	61.9123	34.0051	8.1577
Image 7	84.7866	45.6545	9.7626
Image 8	88.5489	57.1438	9.8422
Image 9	77.6812	33.809	9.8683
Image 10	71.8982	34.4341	7.9564

3.1.4. Absolute Mean Brightness Error

The AMBE results were evaluated for 10 neonatal brain images from three databases and in real time using the three enhancement techniques. Table 4 helps to interpret the trend of the MSE values. The value for BPDFHE is nearly zero, which indicates that it has a low error and yields a more desirable image.

Table 4. Comparison of AMBE values.

S.no.	HE	CLAHE	BPDFHE
Image 1	79.9399	38.1965	0.0768
Image 2	81.0502	40.7308	−0.0759
Image 3	70.306	37.2708	−0.0064
Image 4	30.4979	−2.4163	0.0587
Image 5	70.4643	34.003	0.0312
Image 6	60.0564	24.9076	0.0228
Image 7	81.1538	39.0835	−0.1003
Image 8	94.5837	49.9546	−0.0512
Image 9	75.8575	27.0601	0.0507
Image 10	69.727	26.8082	0.0406

3.2. Segmentation: A Step-Wise ARKFCM Method

- Degree of fuzziness, m = 2 is taken here;
- Median filter is used out of average/weighted filters;
- Iterations are over the ARKFCM objective Function (10), which is given as Equation (10).

3.3. Segmentation Results: With vs. without Preprocessing

The upcoming figures are sectioned into three parts: Each part has an original neonatal brain image, and segmentation is achieved on that image. All the sections were subdivided into two parts—a and b. Part 'a' helps in visualizing tumor detection over the original image (which is not enhanced). On the other hand, part 'b' is of the enhanced image. Figure 10 represents the (a) original image, (b) preprocessed with BPDFHE enhanced image, (c) segmentation result using the median filter, (d) detection of the tumor, and (e) extraction of the tumor using thresholding.

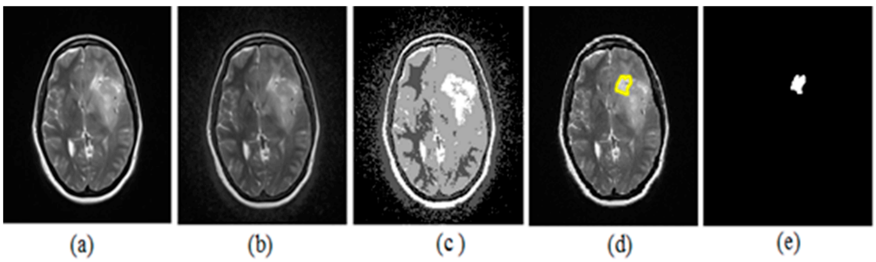

Figure 10. (**a**) Original image, (**b**) BPDFHE enhanced image, (**c**) segmentation result using median filter, (**d**) detection of tumor, and (**e**) extraction of tumor using thresholding.

The estimation of the proposed hybrid method for preprocessing and segmentation using a machine learning algorithm was shown on various MRI images to detect tumors. We placed the images for better visibility after simulations in ink space were used.

Justification of the results was carried out with the dice index (DI) and Jaccard index (JI). The ground truth (GT) image was considered to estimate the performance, which was prepared with the help of a radiologist.

The proposed ARKFCM technique considers spatial information of pixels for processing images which are affected by artifacts such as noise and intensity in-homogeneities. Hence, this procedure includes the effect of neighborhood pixels/voxels aimed at spatial information. Thus, it is capable of extracting boundaries in a proper way when compared to the existing, conventional FCM technique. It was witnessed that the implemented method was able to classify the effects of shielding and bright variations. Therefore, in brief, the main advantages of the proposed method were identified as robust to noise and shielding effects. The computable calculation was performed with Dice Index (DI) and Jaccard Index (JI) metrics [33], processing the difference between the segmented and GT images.

$$Dice\ index = \frac{2|A_i \cap B_i|}{|A_i| + |B_i|} \tag{11}$$

$$Jaccard\ index = \frac{|\ A_i \cap\ B_i|}{|A_i \cup B_i|} \tag{12}$$

Segmentation results of the proposed method are shown in Figures 11 and 12. The obtained numerical values are tabulated in Tables 5 and 6 respectively, including the performance measures of dice similarity and Jaccard index. The proposed method provides efficient and robust results when compared to the FCM technique by a mean of a 98.86% dice index and 96.9% Jaccard index. This helps the physician to check whether the presence of any abnormalities is available in the MRIs corresponding to different parts of the brain. We conclude that the proposed remodified FCM technique ARKFCM method is more robust to noise and shading effects; the major advantage of using this technique is locating the tumor and affected regions.

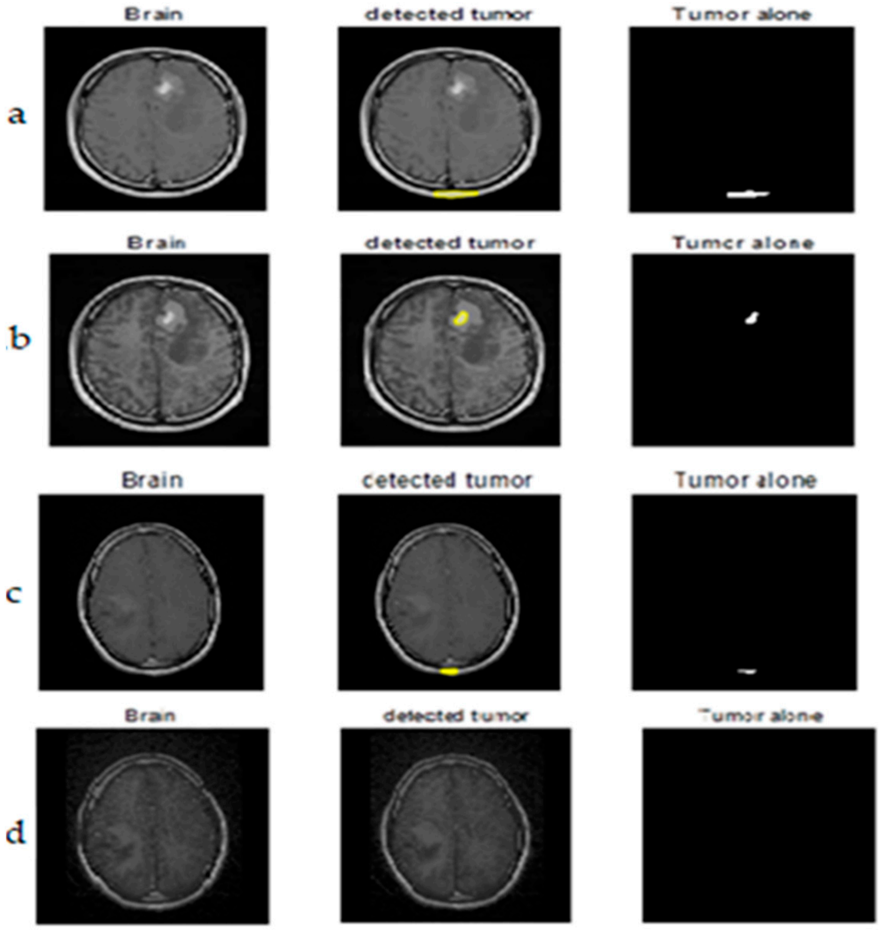

Figure 11. Tumor detection from original MRI brain images. (**a**) the first image in the is the original image, the second image is the segmentation image of the first image after preprocessing, and the third image represents detection of tumor alone. (**b**–**d**) rows consists of original brain images, segmented image with detected tumor, segmented tumor alone with proposed method respectively.

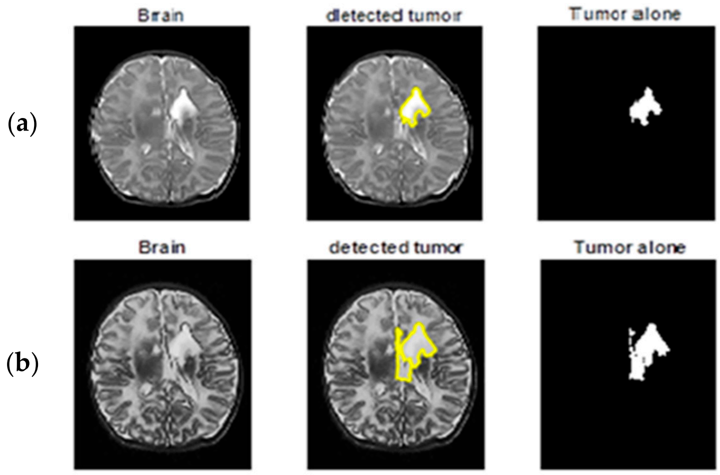

Figure 12. In the figures, the first image in the is the original image, the second image is the segmentation result of the first one, and the third image represents the extraction of the tumor succeeding segmentation. Similarly, in Figure 12, row 2 (**b**), the first figure is the preprocessed result of the original image, and the second and third images are same as above. From the third part, it is visualized with ease that the result of the tumor extraction does have more precision in the case of part '(**b**)' compared to part '(**a**)'.

Table 5. Dice Index with FCM and Proposed ARKFCM method.

Images	FCM	Proposed (ARKFCM)
Figure 10	64.14	99.18
Figure 11a	76.74	98.91
Figure 11b	68.57	98.43
Figure 11c	78.88	99.12
Figure 11d	74.88	99.36
Figure 12a	82.62	98.53
Figure 12b	79.61	98.57

Table 6. Jaccard index with FCM and Proposed ARKFCM method.

Images	FCM	Proposed (ARKFCM)
Figure 10	48.29	97.25
Figure 11a	65.70	97.86
Figure 11b	61.19	95.31
Figure 11c	68.14	93.97
Figure 11d	71.26	99.06
Figure 12a	75.27	96.86
Figure 12b	72.54	96.75

4. Discussions

The identification of brain tumors needs high accuracy and precision; a negligible error can be life-threatening. Brain tumor discovery remains a thought-provoking career in medical image processing. In the proposed work, preprocessing and segmentation methodologies were concentrated to enhance MRI brain tumor detection to help radiologists and patients save time and resources.

In the preprocessing part, the comparison of results after analyzing the preprocessing techniques based on performance metrics (MSE, PSNR, RMSE, and AMBE) was carried out. The MSE value of BPDFHE was lower than the other two, implying it has a low error and yields a more desirable image. The PSNR value improved by 44.95% from HE to CLAHE, and from HE to BPDFHE it improved by 66.9%, and finally, it increased by 84.177% from CLAHE to BPDFHE. The value for BPDFHE was high, which infers it has a low error and yields a more desirable image. The RMSE value of the BPDFHE was less portentous because it had a low error and provided a better-quality image. The value for BPDFHE was nearly zero, which indicates it has a low error and yields a more desirable image.

In the segmentation part, the proposed method provided efficient and robust results when compared to the FCM technique with a mean of 98.86% for the dice index and 96.9% for the Jaccard index because of the degree of fuzziness and reduced number of iterations. This helps physicians to check whether the presence of any abnormalities is available in the MRIs corresponding to different parts of the brain. We conclude that the proposed ARKFCM method, is more robust to noise and shading effects; the major advantage of using this technique is locating the tumor and affected regions with the help of minimized objective function.

5. Conclusions

The detection of brain tumors requires high exactness; a minor error can be life-threatening. Brain tumor disclosure remains a challenging job in medical image processing. In the proposed work, preprocessing and segmentation methodologies were concentrated to enhance tumor detection in MRI brain images to help radiologists and patients save time and resources. Firstly, from the comparative analysis of metrics (PSNR, MSE, RMSE, and AMBE) performed on various preprocessing algorithms, it is concluded from the results obtained that BPDFHE is better than HE or CLAHE. The BPDFHE method evidently showed us with a clear distinction that its PSNR values were higher, MSE and RMSE values were lower, and AMBE values were negligible. This suggests that it has a low error and yields the best quality image. Secondly, the results of segmentation yielded inaccurate results when the images were not preprocessed, and the precision in tumor detection was high, on the other hand, in the case where the images were preprocessed using the ARKFCM method. Hence, image preprocessing is crucial before segmentation is performed, leading to the best results of a 98.86% dice similarity and 96.9% Jaccard index. The proposed ARKFCM method provided the best results.

Author Contributions: Conceptualization, methodology, and validation: S.S. and Y.K.; formal analysis and investigation: G.R.R., S.K., S.M. (Senthilkumar Mohan), H.Q. and S.M. (Saurav Mallik); resources and writing—review: S.S., S.K., S.M. (Senthilkumar Mohan), H.Q. and S.M. (Saurav Mallik); writing—review and editing: Y.K. All authors have read and agreed to the published version of the manuscript.

Funding: H.Q. thanks the USA NSF award 1761839 and 2200138 and a catalyst award from the USA National Academy of Medicine.

Data Availability Statement: https://radiopaedia.org/articles/imaging-data-sets-artificial-intelligence (accessed on 21 April 2021).

Acknowledgments: The authors would like to thank Anusha, a radiologist at Vijaya Diagnostic Centre, Hyderabad, Telangana for the evaluation of the results and valuable suggestions to improve the standard of the article.

Conflicts of Interest: The authors declare no conflict of interest.

References

1. Lakshmi, T.A.; Vinupriyadharshini, R. Noise and skull removal of brain magnetic resonance image using curvelet transform and mathematical morphology. In Proceedings of the 2014 International Conference on Electronics and Communication Systems (ICECS), Coimbatore, India, 13–14 February 2014; pp. 1–4. [CrossRef]
2. Senthilkumaran, N.; Thimmiaraja, J. Histogram equalization for image enhancement using MRI brain images. In Proceedings of the 2014 World Congress on Computing and Communication Technologies, Tiruchirappalli, India, 27 February–1 March 2014; pp. 80–83.
3. Kwon, H.J.; Lee, G.P.; Kim, Y.J.; Kim, K.G. Comparison of pre-processed brain tumor MR images using deep learning detection algorithms. *J. Multimed. Inf. Syst.* **2021**, *8*, 79–84. [CrossRef]
4. Suryavamsi, R.V.; Reddy, L.S.T.; Saladi, S.; Karuna, Y. Comparative Analysis of Various Enhancement Methods for Astrocytoma MRI Images. In Proceedings of the 2018 International Conference on Communication and Signal Processing (ICCSP), Melmaruvathur, India, 3–5 April 2018; pp. 0812–0816.
5. Raj, D.; Mamoria, P. Comparative analysis of contrast enhancement techniques on different images. In Proceedings of the 2015 International Conference on Green Computing and Internet of Things (ICGCIoT), Delhi, India, 8–10 October 2015; pp. 27–31.
6. Saritha, S.; Prabha, N.A. Analysis of denoising filters on MRI brain images. *Int. J. Imaging Syst. Technol.* **2017**, *27*, 201–208.
7. Raghavendra, R.S.; Karuna, Y.; Saladi, S. MS Lesion Segmentation for Single and Multichannel MRI Images Using MICO Technique. In Proceedings of the 2018 International Conference on Communication and Signal Processing (ICCSP), Melmaruvathur, India, 3–5 April 2018. [CrossRef]
8. Despotović, I.; Goossens, B.; Philips, W. MRI Segmentation of the Human Brain: Challenges, Methods, and Applications. *Comput. Math. Methods Med.* **2015**, *2015*, 450341. [CrossRef] [PubMed]
9. Saritha, S.; Prabha, N.A. A comprehensive review: Segmentation of MRI images—Brain tumor. *Int. J. Imaging Syst. Technol.* **2016**, *26*, 295–304. [CrossRef]
10. He, S.; Shen, X.; Yang, Y.; He, R.; Yan, W. Research on MRI brain segmentation algorithm with the application in model-based EEG/MEG. *IEEE Trans. Magn.* **2001**, *37*, 3741–3744. [CrossRef]
11. Xiao, J.; Tong, Y. Research of Brain MRI image segmentation algorithm based on FCM and SVM. In Proceedings of the 26th Chinese Control and Decision Conference (2014 CCDC), Changsha, China, 31 May–2 June 2014; pp. 1712–1716. [CrossRef]
12. Dancea, O.; Tsatos, O.; Gordan, M.; Vlaicu, A. Adaptive fuzzy c-means through support vector regression for segmentation of calcite deposits on concrete dam walls. *Autom. Qual. Test. Robot.* **2010**, *3*, 1–6.
13. Chen, H.; Xie, Z.; Huang, Y.; Gai, D. Intuitionistic fuzzy C-means algorithm based on membership information transfer-ring and similarity measurement. *Sensors* **2021**, *21*, 696. [CrossRef]
14. Alkan, A. Analysis of knee osteoarthritis by using fuzzy c-means clustering and SVM classification. *Sci. Res. Essays* **2011**, *6*, 4213–4219.
15. Yepuganti, K.; Saladi, S.; Narasimhulu, C.V. Segmentation of tumor using PCA based modified fuzzy C means algorithms on MR brain images. *Int. J. Imaging Syst. Technol.* **2020**, *30*, 1337–1345. [CrossRef]
16. Sathya, A.; Senthil, S.; Samuel, A. Segmentation of breast MRI using effective Fuzzy C-Means method based on Support Vector Machine. In Proceedings of the 2012 World Congress on Information and Communication Technologies, Trivandrum, India, 30 October–2 November 2012; pp. 67–72.
17. Elazab, A.; Wang, C.; Jia, F.; Wu, J.; Li, G.; Hu, Q. Segmentation of brain tissues from magnetic resonance images using adaptively regularized kernel-based fuzzy-means clustering. *Comput. Math. Methods Med.* **2015**, *2015*, 485495. [CrossRef]
18. Thejaswini, P.; Bhat, M.B.; Prakash, M.K. Detection and classification of tumour in brain MRI. *Int. J. Eng. Manufact.* **2019**, *9*, 11–20.
19. Iqbal, S.; Ghani, M.U.; Saba, T.; Rehman, A. Brain Tumor Segmentation in Multi-Spectral MRI Using Convolutional Neural Networks (CNN). *Microsc. Res. Tech.* **2018**, *81*, 419–427. [CrossRef] [PubMed]
20. Zhu, Z.; He, X.; Qi, G.; Li, Y.; Cong, B.; Liu, Y. Brain tumor segmentation based on the fusion of deep semantics and edge information in multimodal MRI. *Inf. Fusion* **2023**, *91*, 376–387. [CrossRef]
21. Akkus, Z.; Galimzianova, A.; Hoogi, A.; Rubin, D.L.; Erickson, B.J. Deep learning for brain MRI segmentation: State of the art and future directions. *J. Digit. Imaging* **2017**, *30*, 449–459. [CrossRef]
22. Ullah, Z.; Farooq, M.U.; Lee, S.H.; An, D. A hybrid image enhancement based brain MRI images classification technique. *Med. Hypotheses* **2020**, *143*, 109922. [CrossRef]
23. Saladi, S.; Prabha, N.A. MRI brain segmentation in combination of clustering methods with Markov random field. *Int. J. Imaging Syst. Technol.* **2018**, *28*, 207–216. [CrossRef]
24. Hrosik, R.C.; Tuba, E.; Dolicanin, E.; Jovanovic, R.; Tuba, M. Brain image segmentation based on firefly algorithm combined with k-means clustering. *Stud. Inform. Control* **2019**, *28*, 167–176.
25. Ahmed, M.; Yamany, S.; Mohamed, N.; Farag, A.; Moriarty, T. A modified fuzzy c-means algorithm for bias field estimation and segmentation of MRI data. *IEEE Trans. Med. Imaging* **2002**, *21*, 193–199. [CrossRef]
26. Chen, S.; Zhang, D. Robust image segmentation using FCM with spatial constraints based on new kernel-induced distance measure. *IEEE Trans. Syst. Man Cybern. Part B Cybern.* **2004**, *34*, 1907–1916. [CrossRef]
27. Yang, M.-S.; Tsai, H.-S. A Gaussian kernel-based fuzzy c-means algorithm with a spatial bias correction. *Pattern Recognit. Lett.* **2008**, *29*, 1713–1725. [CrossRef]

28. Krinidis, S.; Chatzis, V. A robust fuzzy local information C-means clustering algorithm. *IEEE Trans. Image Process.* **2010**, *19*, 1328–1337. [CrossRef] [PubMed]
29. Gong, M.; Liang, Y.; Shi, J.; Ma, W.; Ma, J. Fuzzy C-means clustering with local information and kernel metric for image segmentation. *IEEE Trans. Image Process.* **2013**, *22*, 573–584. [CrossRef] [PubMed]
30. Szilagyi, L. Lessons to learn from a mistaken optimization. *Pattern Recognit. Lett.* **2014**, *36*, 29–35. [CrossRef]
31. Lin, W.; Kuo, C.C.J. Perceptual visual quality metrics: A survey. *J. Vis. Commun. Image Represent.* **2011**, *22*, 297–312. [CrossRef]
32. Chen, S.-D.; Ramli, A.R. Minimum mean brightness error bi-histogram equalization in contrast enhancement. *IEEE Trans. Consum. Electron.* **2003**, *49*, 1310–1319. [CrossRef]
33. Bertels, J.; Eelbode, T.; Berman, M.; Vandermeulen, D.; Maes, F.; Bisschops, R.; Blaschko, M.B. Optimizing the dice score and jaccard index for medical image segmentation: Theory and practice. In *International Conference on Medical Image Computing and Computer-Assisted Intervention*; Springer: Cham, Switzerland, 2019; pp. 92–100.